Microchimica Acta
https://doi.org/10.1007/s00604-019-3352-6

ORIGINAL PAPER

An aptasensor for troponin I based on the aggregation-induced electrochemiluminescence of nanoparticles prepared from a cyclometallated iridium(III) complex and poly(4-vinylpyridine-co-styrene) deposited on nitrogen-doped graphene

Mohammad Saremi [1] · Amir Amini [1] · Hamid Heydari [1]

Received: 10 December 2018 / Accepted: 4 March 2019

Abstract

An ultrasensitive electrochemiluminescence (ECL) disposable aptamer sensor (aptasensor) is presented for detection of myocardial infarction biomarker by quantification of troponin I in blood serum. A screen-printed electrode was modified with (a) aptamer-modified gold nanoparticles, (b) cyclometallated iridium(III)-poly-4-vinylpyridine nanoparticles, and (c) nitrogen-doped graphene in order to increase the loading capacity and conductivity of the aptasensor. If the aptasensor is exposed to troponin I, it will bind to the aptamer and desorb the aptamer from gold nanoparticles and the surface of the electrode. This generates an enhancement in ECL emission depending on troponin I concentration. ECL emission is strongly improved by aggregation-induced phenomenon, which is caused by inhibition of the water and oxygen quenching effect on the iridium complex ECL in aqueous media. Under optimum conditions, the aptasensor has a wide dynamic range that extends from 0.1 pM to 10 nM, with a 20 fM detection limit (S/N = 3) and a relative standard deviation of 3.1%. The ECL aptasensor was successfully applied to 20 individual human serum for the detection of troponin I biomarker.

Keywords Biosensor · Aptamer · Carbon screen-printed electrode · Gold nanoparticles · Ionic liquids · Troponin I · Acute myocardial infarction · Cardiovascular diseases · Human serum analysis.

Introduction

Troponin I (TI) is one of the important biomarkers that indicates the acute myocardial infarction (MI) occurrence, as the most life-threatening sorts of cardiovascular diseases, in the human body. In general, elevation in TI concentration in human blood is mostly in concern of MI [1]. In normal people, 0.5 to 2.0 ng.mL^{-1} TI in blood serum is a safe borderline. However, after MI outbreak, TI concentration will raise up to 50 ng.mL^{-1} within 3–6 h, and finally, reach a level around 550 ng.mL^{-1} [2]. This concentration still remains elevated for 6–8 days, which shows a very wide diagnostic window for early detection [3]. Conventional TI detection methods such as mass spectroscopy [4], fluorescence [5] and surface-enhanced Raman spectroscopy [6] suffer from many drawbacks including time-consuming, low sensitivity and high cost.

Electrochemiluminescence (ECL) is a process where excited state luminophores generate at the electrode surface by a high-energy electron transfer reaction [7]. ECL provides many advantages including high sensitivity, good selectivity, low background, wide linear range and low cost which make it a powerful technique in the chemical and biochemical analysis [8]. Hogan and coworkers introduced metallopolymers nanoparticles (MPNPs), such as cyclometallated iridium(III)-polyvinylpyridine polymer nanoparticle (CIPNPs) [9]. CIPNPs showed higher luminescence quantum yield compared to conventional

Electronic supplementary material The online version of this article (https://doi.org/10.1007/s00604-019-3352-6) contains supplementary material, which is available to authorized users.

✉ Amir Amini
amini@wtiau.ac.ir; amir.amini.elec@gmail.com

[1] Department of Electrical Engineering, College of Technical and Engineering, West Tehran Branch, Islamic Azad University, Tehran 1461988631, Iran

Published online: 22 March 2019

$Ru(bpy)_3^{2+}$ in aqueous media [9]. MPNPs also offer aggregation-induced ECL which comes from important protection of cyclometallated iridium(III) complex against quenching process in aqueous media [10]. Therefore, CIPNPs can be used in order to increase ECL intensity resulting in a higher sensitivity of the analysis. In addition, immobilization of ECL luminophore on electrode surface can reduce the costs, enhance ECL signals and simplify the biosensor and bioassay fabrication [11].

Aptamers are single-stranded nucleic acids that can form a 3D specific structure and selectively bind target analyte such as heavy metal ions, nucleic acids, proteins, peptides, cells and micro-organism [12]. Most aptamers obtained through a process called systematic evolution of ligands by exponential enrichment (SELEX) [13]. Aptamers have a small size which has brought many advantages in biosensor and bio-assay technology including high stability, high binding affinity and ease of modifications. Aptamers have grown many attractions and have been widely used in biomolecules detection. Regarding these advantages, numerous papers and book have already been published covering aptamer applications in biosensor and bioassay technology [14].

Nanotechnology is one of the most reliable strategy for sensor fabrication in the chemical and biochemical analysis [15–18]. There are many nanomaterials used in chemical and biochemical sensing applications. Nitrogen-doped graphene (NG) provides many advantages such as high conductivity, good biocompatibility and it is one the superior substrate for biosensor fabrication [19]. It is reported that gold nanoparticles (AuNPs) are among the most utilized nanomaterial for biosensor technology due to their excellent binding with various biological receptors [20]. In addition, Ghasemi et al. have reported improvement of electron transfer by using 1-octyl-3-methylimidazolium hexafluorophosphate (IL) [21]. In particular, significant development has been directed towards the fabrication of ionic liquid-based electrochemical sensing layers.

A novel disposable ECL aptamer sensor (aptasensor) for sensitive detection of TI have constructed. The biosensing platform was fabricated with step by step immobilization of NG, AuNPs-Apt and CIPNPs on carbon screen-printed electrode (CSPE). The aptamer was bound with AuNPs by electrostatic interaction. The synthesis, electrochemical and aptsensor fabrication were characterized using x-ray photoelectron spectroscopy, high angle annular dark-field imaging - transmission electron microscopy, x-ray diffraction spectroscopy, transmission electron microscopy (TEM) and electrochemical impedance spectroscopy (EIS). Finally, the applicability of the aptasensor was investigated in human blood samples and compared with enzyme-linked immunosorbent assay (ELISA).

Experimental

Materials and methods

Potassium hydrogen phosphate (99%), tris(2,2′-bipyridyl)dichlororuthenium(II) hexahydrate (99%), trisodium citrate dehydrate (99%), potassium dihydrogen phosphate (99%), potassium permanganate (99%), sulfuric acid (95%), sodium hydroxide (97%), tripropylamine (TPA) (98%), melamine (99%), iridium chloride hydrate (98%), poly(4-vinylpyridine-co-styrene) (PVPsty) with molecular weight of 10^5 and 1-octyl-3-methylimidazolium hexafluorophosphate (97%) were purchased from Sigma-Aldrich Co (www.sigmaaldrich.com). Tetrachloroauric(III) acid trihydrate (99%), hydrogen peroxide (30%), tetrahydrofuran (99%) (THF), hydrochloric acid (37%) and graphite flakes were purchased from Merck Chemical Co (www.merckmillipore.com). Troponin I, troponin T (TT), troponin C (TC), cytochrome C (CytC), hemoglobin (HEM) and bovine serum albumin (BSA) were also purchased from Sigma-Aldrich Co (www.sigmaaldrich.com). The Aptamer (Apt) with the sequence 5′ –AGTCTCCGCTGTCC TCCCGATGCACTTGACGTATGTCTCACTTTCTTTTC ATTGA-CATGGGATGACGCCGTGACTG - 3′ was prepared by Sinaclon Biotech (Iran) (www.sinaclon.ir). The CV and ECL experiment was performed in the 0.1 M phosphate buffered saline solution with pH 7.4. The ECL luminophore used in this work (CIPNPs) synthesized with iridium precursor complex $[Ir(ppy)_2Cl]_2$ dimers. Synthesis of $[Ir(ppy)_2Cl]_2$ was done according to previous literature [9].

X-ray photoelectron spectroscopy, high angle annular dark-field imaging - transmission electron microscopy, x-ray diffraction spectroscopy and TEM experiment were performed on K-alpha (Thermo Fisher, United Kingdom, www.thermofisher.com) and Jeol JEM-2100F (Tokyo, Japan, www.jeol.co.jp), respectively. EIS experiments were carried out using potentiostat/galvanostate AUTOLAB PGSTAT 30 (Eco Chemie BV, Utrecht, Netherlands, www.metrohm-autolab.com). EIS study was performed to monitor the modification steps of the ECL aptasensor. The EIS measurements were carried out in 1 mM $Fe(CN)_6^{3-/4-}$ containing 0.1 M KCl solution in the frequency range of 100 kHz to 1 mHz and DC amplitude of 10 mV. EIS results were fitted using Levenberg-Marquardt algorithm (with 90% accuracy) in PS Trace software version 5.1 (Palmsense, Netherlands, www.palmsens.com) and results are shown in Table S1. Electrochemical and ECL experiments were performed on 4 mm diameter CSPE manufactured by Dropsense (www.dropsens.com). CSPE consist of carbon working electrode, carbon counter electrode and Ag/AgCl printed reference electrode. ECL measurements were performed in a dark black box. ECL light detector was a Perkin Elmer photoluminescence LS 55 (USA, www.perkinelmer.com) with voltage 800 V.

Synthesis of cyclometallated iridium polymer nanoparticles (CIPNPs)

As reported previously in the literature [9], a cyclometallated iridium polymer (CIP) solution was prepared by mixing 0.41 mM $[Ir(ppy)_2Cl]_2$ and 4 mM PVPsty in THF. Then, to prepare the polymeric nanoparticles, 0.3 mL of the mixture THF solution was flash injected into 6 mL of water under the ultra-sonic bath. The solution was kept under ultra-sonication for 5 min. Then, THF was evaporated by partial vacuum evaporation. The final solution of CIPNPs was utilized for further experiments.

Synthesis of nitrogen-doped graphene (NG)

Synthesis of NG was conducted through thermal annealing of graphite oxide and melamine. Graphite oxide was synthesized according to previously reported literature [19]. Briefly, 3.0 g of graphite was mixed with 70 mL of H_2SO_4. 9.0 g of $KMnO_4$ was added to the solution drop-wisely and then heated to 50 °C for 30 min. 500 mL of deionized water was added to the solution following by addition of 15 mL hydrogen peroxide. The brown solution was filtered and washed with water and HCl solution. The solid was dried in a freeze-drier. The resulting graphite oxide was mixed with melamine (1:5 mass ratio). The mixture was placed in a corundum tube and thermally annealed at 800 °C for 1 h under argon atmosphere. The final solid was cooled down to room temperature and used in further experiments.

Synthesis of gold nanoparticles (AuNPs)

AuNPs was synthesized according to the Turkevich method [22]. Briefly, 20 mL 1 mM of $HAuCl_4$ was placed on a stirring hot plate at 90 °C. Then 2 mL of 1% trisodium citrate was rapidly injected into the solution. The AuNPs gradually forms and the solution becomes deep red. The final solution was kept at 4 °C in a dark refrigerator.

ECL aptasensor fabrication

The ECL aptasensor was fabricated as presented in Fig. 1. In the first step, CSPE was pretreated by applying 10 potential sweeps ranging from 0.9 to 1.5 V in various electrolyte solutions including 1 M H_2SO_4, 1 M $NaHCO_3$ and 1 M Na_2CO_3. Electrochemical pretreatment helped to remove organic contaminants and increases surface roughness [23]. After electrochemical pretreatment, CSPE was rinsed with deionized water and dried with N_2 gas (99.999% pure). In the next step, 5 μL of an aqueous solution containing 1 $mg.mL^{-1}$ NG was drop casted on the CSPE surface and dried at room temperature. A solution of 1 μM aptamer adsorption on AuNPs was carried out for 1 h at 37 °C through electrostatic interaction. Then, CIPNPs solution was mixed with IL and AuNPs-Apt solution (1:1:3 v:v:v). Then, 5 μM of the resulting suspension was dropped on CSPE/NG. The CSPE/NG/CIPNPs-IL-AuNPs-Apt electrode was kept at room temperature for 30 min to evaporate the excess water. The electrode was rinsed with 0.1 M phosphate buffer saline solution with pH 7.4 and incubated in BSA for 1 h to block non-specific binding sites. The aptasensor was washed with deionized water and stored at 4 °C in a dark refrigerator. In order to perform a comparative study, the same procedure was applied to prepare CSPE/NG/$Ru(bpy)_3^{2+}$-IL-AuNPs and CSPE/NG/CIPNPs-IL-AuNPs.

ECL measurement of troponine I (TI)

The ECL aptasensor was incubated in a various concentration of TI for 1 h at 37 °C. Then the aptasensor was rinsed with 0.1 M phosphate buffer saline solution with pH 7.4 and deionized water, respectively. Afterward, the ECL measurements were performed over a scan range of 0–1.2 V vs Ag/AgCl in 0.1 M phosphate buffer saline solution with pH 7.4 containing 5 mM TPA. The selectivity of the aptasensor was investigated in the same condition in presence of 100 pM HEM, 100 pM CytC, 100 pM BSA, 100 pM TC and 100 pM TT.

ELISA procedure for patient samples

Human blood samples were obtained from 20 persons. Blood samplings were carried out in a clinical lab, Bouali Hospital, Sari, Iran (www.bouali.iautmu.ac.ir). TI concentration in all 20 samples determined by the ELISA procedure. ELISA was performed in 96-well plates coated with streptavidin. After plotting a typical calibration plot, each serum was extracted and TI concentrations were measured by the ELISA kit. The extracted serum samples were diluted with 0.1 M phosphate buffer saline solution with pH 7.4 (in order to place within the linear range of the ECL aptasensor) and the ECL aptasensor was applied to samples.

Result and discussion

Characterization of nitrogen-doped graphene (NG)

TEM images of NG are displayed in Fig. 2a. Figure 2a shows the typical structure of NG, the single thin and compact planar sheets of NG are well separated and associated with each other. This morphology indicated a high surface to volume ratio of NG. Also, the structure of prepared NG was characterized by XRD. The XRD pattern of the NG was investigated

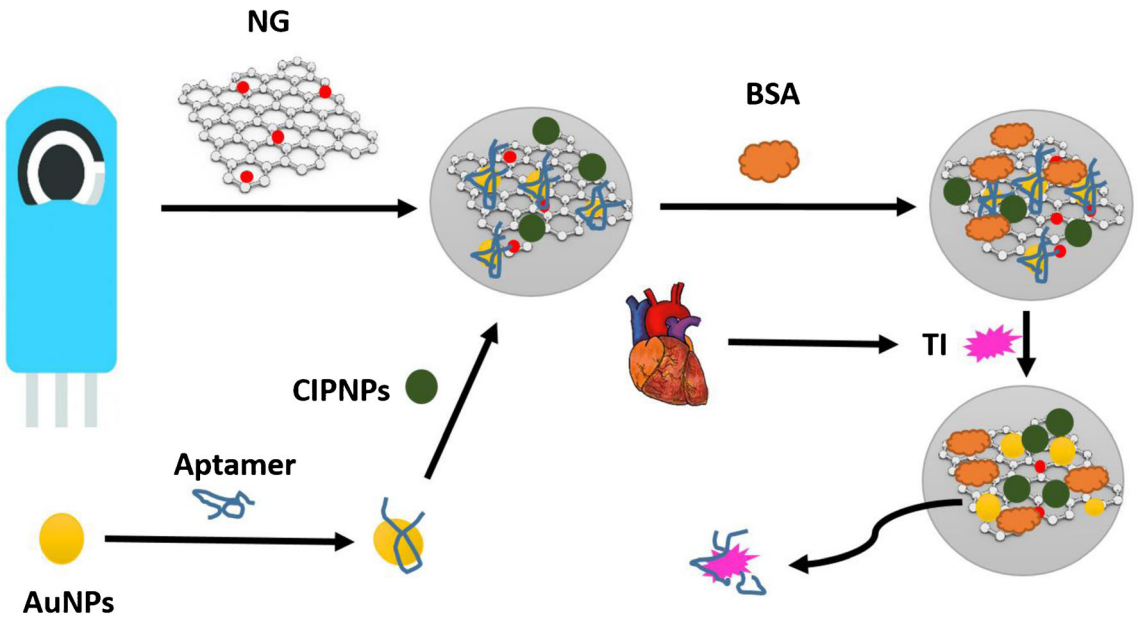

Fig. 1 ECL aptasensor fabrication procedure

and compared with literature (Fig. 2b). As shown in Fig. 2b, a broad peak at 2θ = 26° and a small peak at 2θ = 42° attributed to graphite and graphite-like structure. The absence of a peak at 2θ = 12° suggest the successful reduction of GO by thermal annealing procedure. Clearly, the conformation of NG is confirmed with the previous reports.

Raman spectroscopy is a useful method to characterize NG. In Fig. 2c, the D, G, and 2D bands are shown at around 1320–1350, 1570–1585 and 2640–2680 cm^{-1}, respectively. The G band corresponds to doubly degenerate E_{2g} phonons at the Brillouin zone. The D band with A_{1g} symmetry represents the sp^2C with defects which confirms the edge defects, dangling bonds, vacancies and topological defects.

The FTIR spectra of NG is presented in Fig. 2d. As shown in Fig. 2d, a weak peak at around 1742 cm^{-1} corresponds to C = O groups. C – C and C – O stretching peaks are observed at 1160 and 1032 cm^{-1}. In addition, the peak at 1556 cm^{-1} assigned to the superposition of the vibration of C = N bond, which is the evidence of nitrogen doping in graphene structure.

X-ray photoelectron spectroscopy is the most important technique to investigate nitrogen doping in graphene structure. In x-ray photoelectron spectra (Fig. 2e), three major peaks at 287 eV, 400 eV and 533 eV representing carbon 1 s, nitrogen 1 s and oxygen 1 s is observed, respectively. The carbon 1 s region includes C – C (284.6 eV), C – OH (285.8 eV), C = O (287.1 eV), C – N (289.1 eV). The nitrogen 1 s region can be divided into three peaks at 397 eV, 399 eV and 401 eV representing pyridinic, pyrolytic and graphitic nitrogen in NG structure, respectively. In addition, peaks at 532.5 eV and 533.9 eV assigned to C = O and C – OH bonds. These results clearly prove the doping of nitrogen atoms in NG structure. In addition, high angle annular dark field-TEM elemental map (Fig. 2f) shows the homogeneous doping of nitrogen in NG nano-sheets. All of these findings suggest an appropriate synthesis of NG by the thermal annealing method.

AuNP synthesis and aptamer adsorption

TEM images of AuNPs are shown in Fig. S1. It can be seen that the average size of colloidal AuNPs are 18 nm. Also, the UV-Vis spectrum of AuNPs shows an absorption peak at 520 nm (Fig. S2). AuNPs are known for their distinct optical feature referred to localized surface Plasmon resonance (LSPR) which results in a strong absorption at around 500–600 nm [24]. Zeta potential measured for AuNPs, aptamer and AuNPs-Apt. Zeta potential for AuNPs, aptamer and AuNPs-Apt were + 24.2 mV, −18.3 mV and + 4.6 mV, respectively (Fig. S3). The positively charged AuNPs and negatively charged aptamer can support the electrostatic adsorption of aptamer on the surface of AuNPs.

In order to prove the electrostatic adsorption of the aptamer on the surface of AuNPs, TEM and UV-Vis spectroscopy have been performed. When an appropriate amount of NaCl added to the AuNPs solution, the LSPR UV-Vis absorption peak decreased gradually (Fig. S4). These changes indicate AuNPs aggregation in presence of salt induction. However, by addition of NaCl to AuNPs-Apt solution, LSPR UV-Vis absorption peak shows a negligible change (Fig. S4). This result suggests that aptamer serves as a stabilizer and prevents AuNPs salt-induced aggregation [25]. Also, TEM images show salt-induced aggregation of AuNPs in the solution without addition of aptamer (Fig. S5). On the contrary, the addition of NaCl to the AuNPs-Apt solution shows no salt-

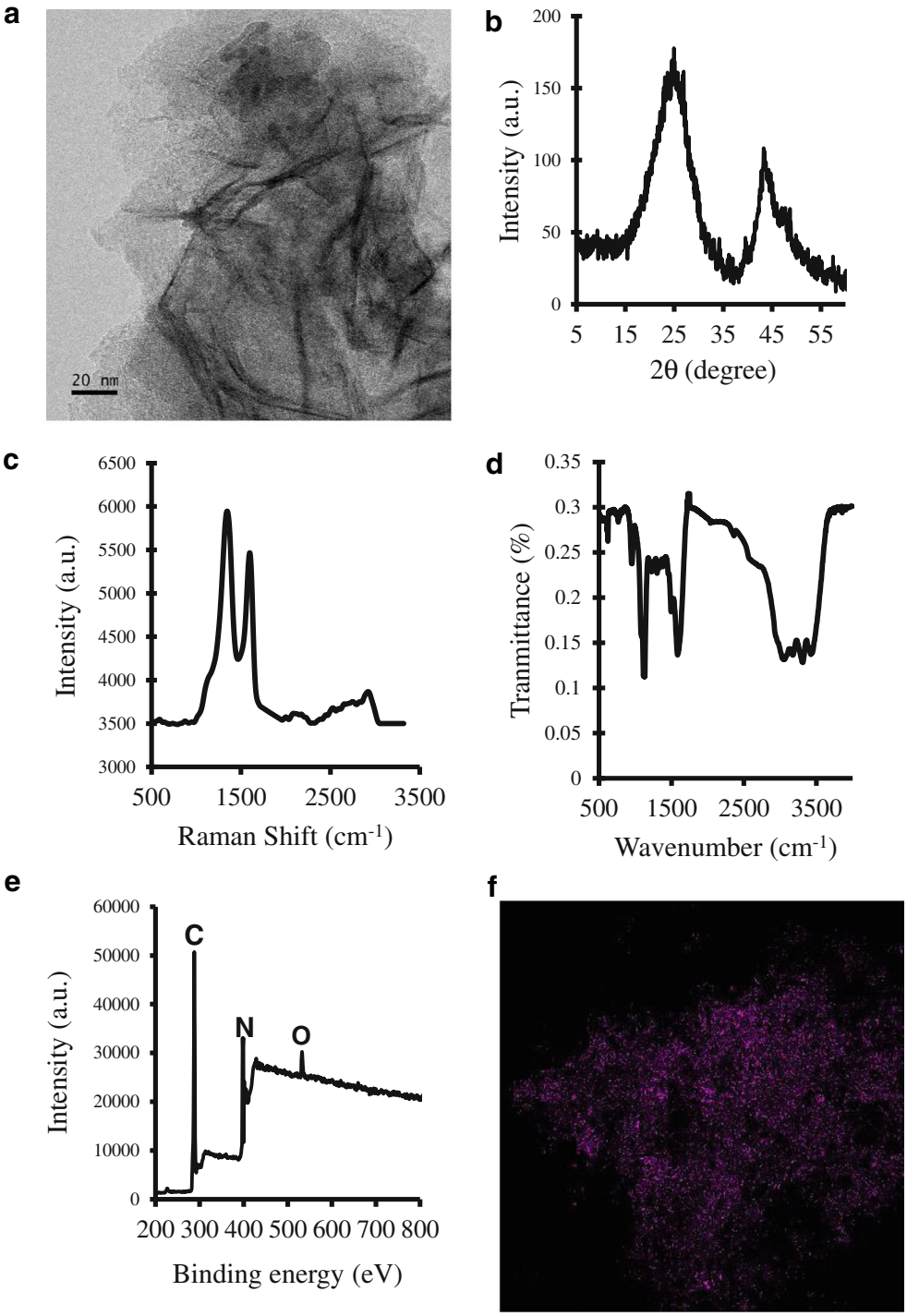

Fig. 2 TEM image (**a**), x-ray diffraction spectra (**b**), Raman spectrum (**c**), FTIR spectrum (**d**) and x-ray photoelectron spectrum (**e**) of NG. High angel annular dark field-TEM map of nitrogen doping (purple dots) in NG (f)

induced aggregation (Fig. S5). Therefore, it is presumed that the aptamer was successfully adsorbed on the surface of the AuNPs.

Synthesis of cyclometallated iridium(III) -polyvinylpyridine polymer nanoparticles (CIPNPs)

TEM images (Fig. 3a) shows a spherical morphology of the CIPNPs with an average size of 43 nm. The photoluminescence and UV-Vis measurements (Fig. 3b, c) reveals that the absorption spectrum in relatively broad and without any unique features, indicating scattering effect. Meanwhile, the emission profile is much higher than CIP in THF media. This indicates that LLCT/MLCT transitions are not affected by the quenching effects including solvent and oxygen. In fact, the aggregation of the iridium complex causes significant protection against water and oxygen quenching effects. This exceptional improvement for CIPNPs is due to aggregation-induced ECL

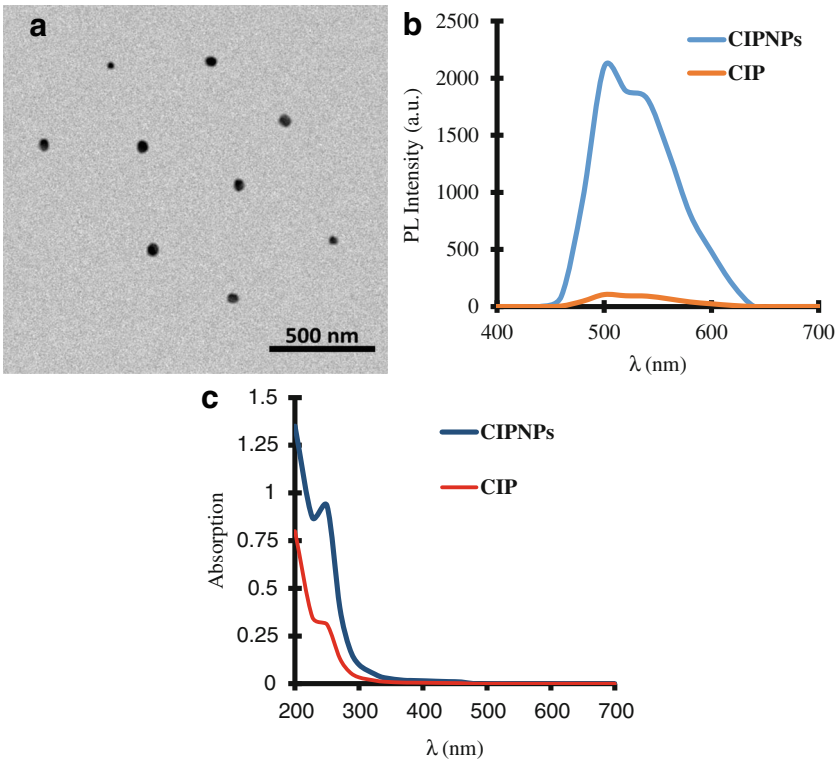

Fig. 3 TEM image of CIPNPs (**a**), PL emission spectrum of CIP and CIPNPs (**b**) and UV-Vis spectrum of CIP and CIPNPs (**c**)

where the PVPsty aggregates in water and protect the emitting centers from quenching agents in aqueous media [9].

Electrochemical characterization of the aptasensor

Prior to the EIS study, the effective surface area of the electrode was calculated using the Randles-Sevcik equation:

$$I_p = \left(2.69 \times 10^5\right) n^{3/2} A D_0^{1/2} C_0^* \nu^{1/2} \quad (1)$$

Where ν is the sweep rate of potential, A is the effective surface area, D_0 is the diffusion coefficient, C_0* is the probe concentration, n is the number of the electron transferred in the redox reactions and I_p is the peak current of the redox couple. The effective surface area (A) is proportional to $I_p/\nu^{1/2}$. Cyclic voltammograms of the CSPE and modified CSPE were performed in a solution containing 0.1 M KCl and 10 mM $K_3Fe(CN)_6$ at different potential sweep rates. The effective surface area of the electrodes were extrapolated from the Randles-Sevcik equation [26] and summarized in Table S2.

The EIS Nyquist plots and the equivalent circuit are presented in Fig. 4a, b. At high frequencies, the CSPE exhibits a semicircle domain relating to capacitance and charge transfer resistance (R_{ct}). The bare CSPE shows a small R_{ct} (405 Ω) indicating a fast electron transfer process of the probe. Modification of the bare CSPE by NG decreases the R_{ct} (302 Ω) but increases the capacitance impedance of the electrode which is related to electrochemical double layer of the electrode surface. In Table S1, it can be seen that by modifying the electrode surface with NG, the effective surface area of the electrode increases from 7.2 mm^2 to 26.3 mm^2, which is in consistent with EIS results. This is explained by excellent conductivity and high surface area of NG. The next step is the modification of the CSPE/NG surface by CIPNPs-IL-AuNPs-Apt which increases the R_{ct} (1168 Ω). This demonstrates the electron transfer prevention by aptamer on the surface of the electrode. Also, the Table S2 shows a slight improvement of the effective surface area of the electrode after modification with CIPNPs-IL-AuNPs-Apt which is related to the presence of AuNPs on surface of the electrode. The incubation of BSA on the electrode causes further increase to R_{ct} (1823 Ω) and reduce the effective surface area of the electrode. This can be explained that BSA blocks non-specific site of the electrode surface and reduce the effective surface area of the electrode. By addition of TI to the solution, the R_{ct} decreases (869 Ω), which demonstrates that aptamer sequences successfully binds to TI and releases from the surface of the electrode.

ECL performance of the aptasensor

The ECL emission of CIPNPs compared with the benchmark $Ru(bpy)_3^{2+}$ in the 0.1 M phosphate buffer saline

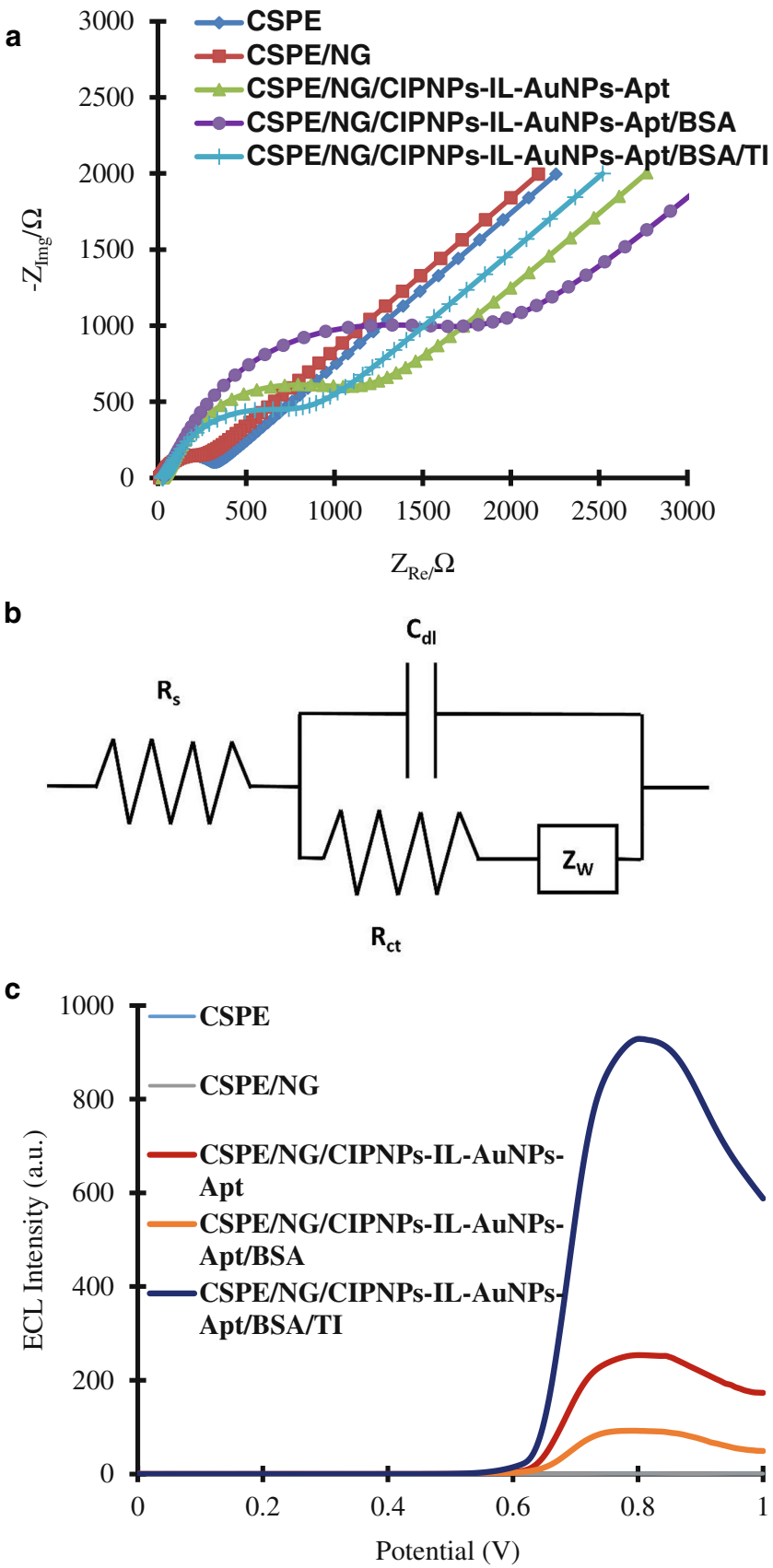

Fig. 4 Nyquist plot of ECL aptasensor in each modification step in 1 mM $Fe(CN)_6^{3-/4-}$ containing 0.1 M KCl solution (**a**) and the equivalent circuit (**b**). The ECL signal of ECL aptasensor in each modification step in 0.1 M phosphate buffer saline solution pH 7.4 solution containing 1 mM TPA (**c**)

solution with pH 7.4 containing 0.1 mM TPA (Fig. S6). Two electrodes fabricated without aptamer, first CSPE/NG/ $Ru(bpy)_3^{2+}$-IL-AuNPs and the other one was CSPE/NG/ CIPNPs-IL-AuNPs. The ECL emission of both electrodes is shown in Fig. S6. It can be seen that the ECL emission of CSPE/NG/CIPNPs-IL-AuNPs is 15 times higher than CSPE/NG/ $Ru(bpy)_3^{2+}$-IL-AuNPs. It is reported that iridium-based luminophores have many favorable attributes such as high quantum yields and lifetime [27]. Despite that, application of iridium-based luminophores is limited due to their poor performance in aqueous media [10]. The superiority of CIPNPs over benchmark $Ru(bpy)_3^{2+}$ in aqueous media arises from aggregation-induced ECL which protects the CIPNPs from quenching effects. These results confirm that CIPNPs proves to be much more sensitive ECL probe than benchmark $Ru(bpy)_3^{2+}$. The ECL mechanism of iridium-based luminophores has been extensively studied in the literature [28] and represented as follows:

$$Ir(ppy)_3 - e^- \rightarrow Ir(ppy)_3^+$$

$$TPA - e^- \rightarrow [TPA^\bullet]^+ \rightarrow TPA^\bullet + H^+$$

$$Ir(ppy)_3^+ + TPA^\bullet \rightarrow Ir(ppy)_3^* + \text{products}$$

$$Ir(ppy)_3^* \rightarrow Ir(ppy)_3 + h\nu$$

The ECL behavior of the ECL aptasensor was studied in each modification process and the results are shown in Fig. 4c. The ECL measurements and linear sweep voltammetry (LSV) were performed simultaneously. LSV experiment was carried out in potential range 0–1 V with the sweep rate of 50 $mV.s^{-1}$ in the 0.1 M phosphate buffer saline solution with pH 7.4 containing 1 mM TPA as ECL coreactant. The bare CSPE and CSPE/NG shows no ECL signal. After modification of CSPE/NG with CIPNPs-IL-AuNPs-Apt, an obvious ECL signal can be observed. This can be explained by inert electron transfer of the aptamer and BSA. Finally, TI addition dramatically increases the ECL signal. TI interaction with aptamer is stronger than electrostatic adsorption of aptamer on the surface of AuNPs. Therefore, TI binds to aptamer and desorbs the aptamer from the surface of the AuNPs and electrode. This causes an improvement in the oxidation of ECL reagent species on the electrode surface and also the ECL intensity. These results confirm the high specific affinity of the aptamer toward the TI biomarker. This enhancement in ECL signal was used as a detection strategy for determination of TI.

Optimization of the method

The main parameters affecting the performance of ECL aptasensor were optimized. These parameters include TPA concentration, aptamer adsorption time and TI incubation time. Respective data and figures are shown in the electronic supplementary information (Fig. S7–10). The optimum conditions were pH 7.4, 1 mM TPA, 1 h adsorption time and 1 h incubation time and used for further experiments.

Analytical performance of the ECL aptasensor

Under the optimum conditions, the ECL aptasensor response shows a linear relationship with TI concentration logarithm from 0.1 pM to 10 nM with the detection limit of 0.02 pM ($S/N = 3$) with the relative standard deviation (RSD) of 3.1% ($n = 10$ for blank solution) (Fig. 5a, b). The correlation equation for ECL intensity and TI concentration were $I = 2220.30 + 157.11\ LogC_{TI}$ with the regression coefficient of 0.9974 (Fig. 5b). In addition, the reproducibility of the ECL aptasensor was investigated for 5 separately fabricated aptasensor in consecutive days. Each aptasensor was prepared in 5 different consecutive days and applied to 0.1 M phosphate buffer saline solution with pH 7.4 containing 0.1 pM TI at the same day. Also, it should be noted that each sample solutions were prepared daily. The respective ECL intensities are shown in Fig. 5c. The RSD value of the 5 individual ECL aptasensor was 2.5%, suggesting the reproducible performance of the aptasensor.

The analytical performance of the ECL aptasensor was compared with previously reported literature in Table 1 [29–35]. The performance of the ECL aptasensor toward detection of TI is superior compared to most of the previous studies. Also, method offer using aptamer as bio-receptor which is, at least in this case, easier to utilize compared to antibody bio-receptors. This suggests that the ECL aptasensor possess high potential for TI detection.

The selectivity of the ECL aptasensor was also studied in the presence of HEM, CytC, BSA, TT, TC in a solution containing 0.1 pM TI. The results are shown in Fig. 5d. It can be seen that in the presence of 100 pM of various interferences, there is a negligible change in ECL intensity. This shows a high affinity of aptamer toward TI which causes high selectivity of the ECL aptasensor.

Regarding the analytical performance of ECL aptasensor, it is verified that the ECL aptasensor can be nominated as an ultrasensitive method for determination of TI. Moreover, the ECL aptasensor can perform ultrasensitive detection of TI without any significant interference effect. Also, a comparison study was performed between IL, chitosan and Nafion as immobilizer of cyclometallated iridium(III)-polyvinylpyridine polymer nanoparticles (CIPNPs) and AuNPs on the surface of the electrode (see S2 and Fig. S11). Immobilizing the

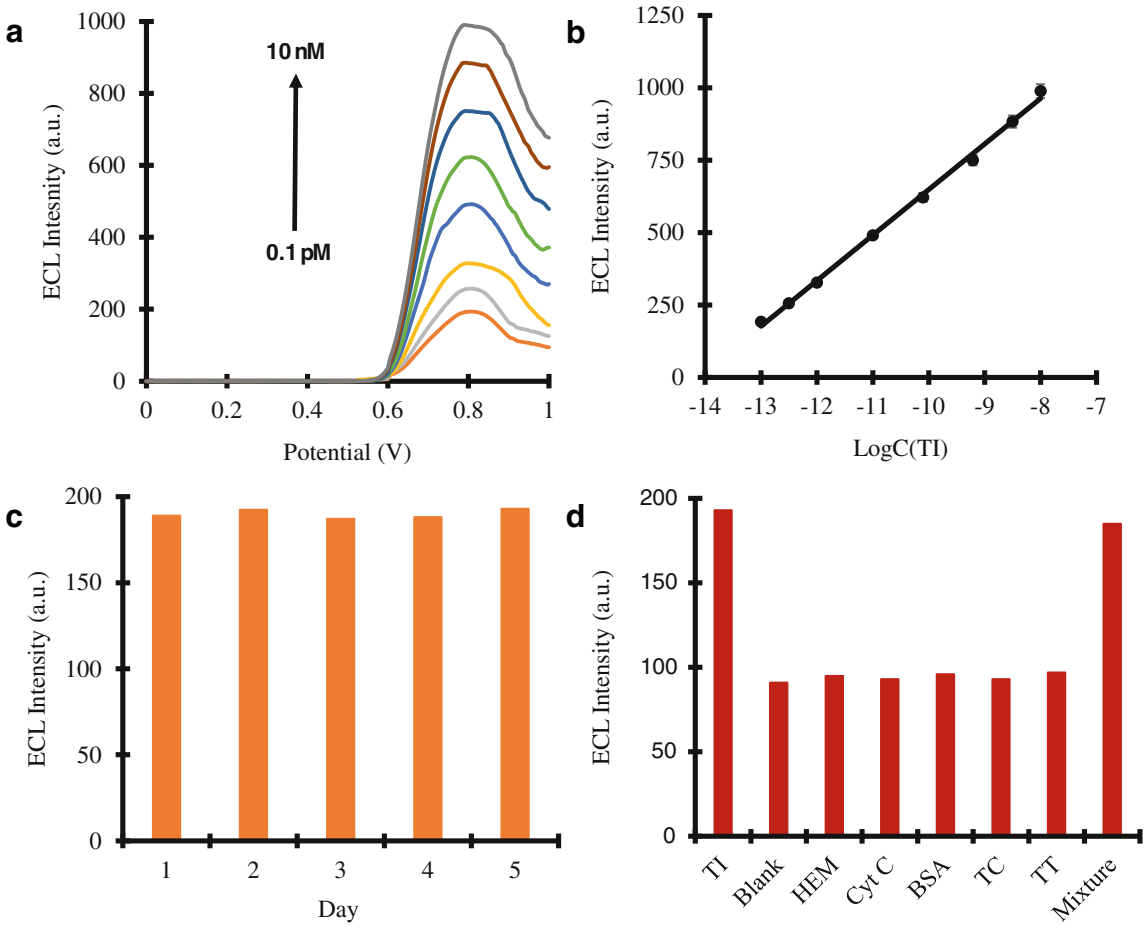

Fig. 5 The ECL signals of 0.1 pM, 3.15 pM, 10 pM, 100 pM, 800 pM, 0.62 nM, 3.2 nM and 10 nM pM of TI in 0.1 M phosphate buffer saline solution pH 7.4 containing 1 mM TPA (**a**) and respective calibration plot (**b**). The ECL aptasensor response for 0.1 pM TI in 5 consecutive days(**c**). Effect of common interference (100 pM) on ECL aptasensor performance for detection of 0.1 pM TI (**d**)

CIPNPs and AuNPs on the surface of the electrode by IL provides a slightly higher ECL emission compared to the other two. Therefore, IL was selected for aptasensor fabrication. In the next step, the ECL aptasensor was used for detection of TI in real samples.

Application of the ECL aptasensor in early detection of TI

The ECL aptasensor was employed for the detection of TI in human. Blood serum samples of 20 healthy persons

Table 1 Comparison between other methods for determination of cardiac biomarker TI

Method	Bio-receptor	Signal generation	Dynamic range	Detection limit	Ref
Chronoamperometry	Aptamer	Catalytic reaction between hydrazine and H_2O_2	1–100 pM	1 pM	[29]
Differential pulse voltammetry	Aptamer	Oxidation of $[Fe(CN)_6]^{4-}$	1–1100 pM	0.18 pM	[30]
ECL	DNA	Ferrocene	100 pM – 1 μM	0.016 pM	[31]
Colorimetric	Aptamer	Biotin – aptamer and streptavidin–AuNPs based dot blot assay	5–100 $ng.mL^{-1}$	5 $ng.mL^{-1}$	[32]
Colorimetric	Antibody	Darkness of silver deposition was relative to the amount of antigen	0.01–10 $ng.mL^{-1}$	0.01 $ng.mL^{-1}$	[33]
Differential pulse voltammetry	Aptamer	Oxidation of $[Fe(CN)_6]^{4-}$	1 $pg.mL^{-1}$ – 100 $ng.mL^{-1}$	1 pg mL^{-1}	[34]
Photoelectrochemical sensor	Antibody	Graphene quantum dot doped with nitrogen and sulfur	0.001 $ng.mL^{-1}$ – 50 $ng.mL^{-1}$	0.3 $pg.mL^{-1}$	[35]
ECL	Aptamer	CIPNPs	0.1 pM – 10 nM	0.02 pM	Current work

Table 2 The TI level in human samples detected by ELISA and ECL aptasensor

Sample number	TI level using ELISA ($ng.mL^{-1}$)	TI level using ECL aptasensor ($ng.mL^{-1}$)	Condition
1	0.3	0.31	negative
2	0.1	0.13	negative
3	0.2	0.22	negative
4	0.2	0.21	negative
5	0.4	0.41	negative
6	0	0.01	negative
7	0.3	0.31	negative
8	0.4	0.43	negative
9	2.3	2.35	positive
10	4.1	4.41	positive
11	0.7	0.79	positive
12	1.3	1.42	positive
13	2.6	2.71	positive
14	4.5	4.55	positive
15	0.8	0.88	positive
16	9.1	9.21	positive
17	5.3	5.32	positive
18	4.3	4.31	positive
19	0.9	0.96	positive
20	3.2	3.31	positive

and patients were analyzed with both ELISA kit and the ECL aptasensor. The quantitative levels of TI in all samples are shown in Table 2. The ECL aptasensor successfully managed to successfully differentiate between healthy persons and patients.

Conclusion

In summary, a novel ECL aptasensor for early detection of MI based on quantification of TI was introduced. The ECL aptasensor shows high sensitivity and selectivity toward label-free determination of TI in human blood serum. The NG effectively increases the loading capacity of CIPNPs on the surface of the electrode. CIPNP shows much higher ECL intensity compared to benchmark $Ru(bpy)_3^{2+}$ due to aggregation-induced ECL phenomenon and great ECL properties of the iridium-based complex. Furthermore, due to the critical importance of the MI early diagnosis, fabrication of TI bioassay is a crucial achievement in health science. This method can be nominated as an alternative method to other conventional method for detection of TI.

Compliance with ethical standards There are no conflicts to declare.

References

1. Sheng Q, Qiao X, Zhou M, Zheng J (2017) Recent progress in electrochemical sensing of cardiac troponin by using nanomaterial-induced signal amplification. Microchim Acta 184(6):1573–1585. https://doi.org/10.1007/s00604-017-2219-y
2. Fathil M, Arshad MM, Gopinath SC, Hashim U, Adzhri R, Ayub R, Ruslinda A, Nuzaihan M, Azman A, Zaki M (2015) Diagnostics on acute myocardial infarction: cardiac troponin biomarkers. Biosens Bioelectron 70:209–220. https://doi.org/10.1016/j.bios.2015.03.037
3. Wu AH, Apple FS, Gibler WB, Jesse RL, Warshaw MM, Valdes R (1999) National Academy of Clinical Biochemistry standards of laboratory practice: recommendations for the use of cardiac markers in coronary artery diseases. Clin Chem 45(7):1104–1121
4. Schneck NA, Phinney KW, Lee SB, Lowenthal MS (2018) Quantification of cardiac troponin I in human plasma by immunoaffinity enrichment and targeted mass spectrometry. Anal Bioanal Chem 410(11):2805–2813. https://doi.org/10.1007/s00216-018-0960-7
5. Li Y, Dai W, Lv X, Deng Y (2018) Aptamer-based rolling circle amplification coupled with graphene oxide-based fluorescence resonance energy transfer for sensitive detection of cardiac troponin I. Anal Methods 10(15):1767–1773. https://doi.org/10.1039/C8AY00309B
6. Chon H, Lee S, Yoon S-Y, Lee EK, Chang S-I, Choo J (2014) SERS-based competitive immunoassay of troponin I and CK-MB markers for early diagnosis of acute myocardial infarction. Chem Commun 50(9):1058–1060. https://doi.org/10.1039/C3CC47850E
7. Miao W (2008) Electrogenerated chemiluminescence and its biorelated applications. Chem Rev 108(7):2506–2553. https://doi.org/10.1021/cr068083a
8. Li S, Liu C, Han B, Luo J, Yin G (2017) An electrochemiluminescence aptasensor switch for aldicarb recognition via ruthenium complex-modified dendrimers on multiwalled carbon nanotubes. Microchim Acta 184(6):1669–1675. https://doi.org/10.1007/s00604-017-2177-4
9. Carrara S, Stringer B, Shokouhi A, Ramkissoon P, Agugiaro J, Wilson DJD, Barnard PJ, Hogan CF (2018) Unusually strong Electrochemiluminescence from iridium-based redox polymers immobilized as thin layers or polymer nanoparticles. ACS Appl Mater Interfaces 10(43):37251–37257. https://doi.org/10.1021/acsami.8b12995
10. Moghaddam MR, Carrara S, Hogan CF (2019) Multi-colour bipolar electrochemiluminescence for heavy metal ion detection. Chem Commun 55(8):1024–1027. https://doi.org/10.1039/C8CC08472F
11. Lu L, Wu J, Li M, Kang T, Cheng S (2015) Detection of DNA damage by exploiting the distance dependence of the electrochemiluminescence energy transfer between quantum dots and gold nanoparticles. Microchim Acta 182(1):233–239. https://doi.org/10.1007/s00604-014-1322-6
12. Liu Y, Yu J (2016) Oriented immobilization of proteins on solid supports for use in biosensors and biochips: a review. Microchim Acta 183(1):1–19. https://doi.org/10.1007/s00604-015-1623-4
13. Wu J, Zhu Y, Xue F, Mei Z, Yao L, Wang X, Zheng L, Liu J, Liu G, Peng C (2014) Recent trends in SELEX technique and its application to food safety monitoring. Microchim Acta 181(5–6):479–491. https://doi.org/10.1007/s00604-013-1156-7
14. Xu Q, Wang G, Zhang M, Xu G, Lin J, Luo X (2018) Aptamer based label free thrombin assay based on the use of silver nanoparticles incorporated into self-polymerized dopamine. Microchim Acta 185(5):253. https://doi.org/10.1007/s00604-018-2787-5
15. Amini A, Hosseini-Golgoo SM (2012) Rapid recognition of airborne combustible molecules with an operating temperature-modulated gas sensor. Sens Lett 10(3–4):821–825. https://doi.org/10.1166/sl.2012.2571

16. Jafari A, Amini A (2019) Lactic acid gas sensor based on polypyrrole thin film. Mater Lett 236:175–178. https://doi.org/10.1016/j.matlet.2018.10.066
17. Hossein-Babaei F, Masoumi S, Noori A (2018) Linking thermoelectric generation in polycrystalline semiconductors to grain boundary effects sets a platform for novel Seebeck effect-based sensors. J Mater Chem A 6(22):10370–10378. https://doi.org/10.1039/C8TA02732C
18. Hossein-Babaei F, Moghadam S, Masoumi S (2015) Forming ohmic Ag/SnO_2 contacts. Mater Lett 141:141–144. https://doi.org/10.1016/j.matlet.2014.11.046
19. Wang Y, Shao Y, Matson DW, Li J, Lin Y (2010) Nitrogen-doped graphene and its application in electrochemical biosensing. ACS Nano 4(4):1790–1798. https://doi.org/10.1021/nn100315s
20. Jiao XX, Chen JR, Zhang XY, Luo HQ, Li NB (2013) A chronocoulometric aptasensor based on gold nanoparticles as a signal amplification strategy for detection of thrombin. Anal Biochem 441(2):95–100. https://doi.org/10.1016/j.ab.2013.07.023
21. Moghaddam MR, Norouzi P, Ghasemi JB (2018) Simultaneous sensitive determination of benzenediol isomers using multiwall carbon nanotube–ionic liquid modified carbon paste electrode by a combination of artificial neural network and fast Fourier transform admittance voltammetry. New J Chem 42(8):6479–6487. https://doi.org/10.1039/C7NJ04073C
22. Kimling J, Maier M, Okenve B, Kotaidis V, Ballot H, Plech A (2006) Turkevich method for gold nanoparticle synthesis revisited. J Phys Chem B 110(32):15700–15707. https://doi.org/10.1021/jp061667w
23. Pur MRK, Hosseini M, Faridbod F, Ganjali MR (2017) Highly sensitive label-free electrochemiluminescence aptasensor for early detection of myoglobin, a biomarker for myocardial infarction. Microchim Acta 184(9):3529–3537. https://doi.org/10.1007/s00604-017-2385-y
24. Eustis S, El-Sayed MA (2006) Why gold nanoparticles are more precious than pretty gold: noble metal surface plasmon resonance and its enhancement of the radiative and nonradiative properties of nanocrystals of different shapes. Chem Soc Rev 35(3):209–217. https://doi.org/10.1039/B514191E
25. Wei H, Li B, Li J, Wang E, Dong S (2007) Simple and sensitive aptamer-based colorimetric sensing of protein using unmodified gold nanoparticle probes. Chem Commun (36):3735–3737. https://doi.org/10.1039/B707642H
26. Allibai Mohanan VM, Kacheri Kunnummal A, Biju VMN (2016) Electrochemical sensing of hydroxylamine using a wax impregnated graphite electrode modified with a nanocomposite consisting of ferric oxide and copper hexacyanoferrate. Microchim Acta 183(6):2013–2021. https://doi.org/10.1007/s00604-016-1839-y
27. Haghighatbin MA, Laird SE, Hogan CF (2018) Electrochemiluminescence of cyclometalated iridium (III) complexes. Curr Opin Electrochem 7:216–223. https://doi.org/10.1016/j.coelec.2018.03.026
28. Kim JI, Shin I-S, Kim H, Lee J-K (2005) Efficient electrogenerated chemiluminescence from cyclometalated iridium (III) complexes. J Am Chem Soc 127(6):1614–1615. https://doi.org/10.1021/ja043721x
29. Jo H, Her J, Lee H, Shim Y-B, Ban C (2017) Highly sensitive amperometric detection of cardiac troponin I using sandwich aptamers and screen-printed carbon electrodes. Talanta 165:442–448. https://doi.org/10.1016/j.talanta.2016.12.091
30. Lopa NS, Rahman MM, Ahmed F, Ryu T, Sutradhar SC, Lei J, Kim J, Kim DH, Lee YH, Kim W (2019) Simple, low-cost, sensitive and label-free aptasensor for the detection of cardiac troponin I based on a gold nanoparticles modified titanium foil. Biosens Bioelectron 126:381–388. https://doi.org/10.1016/j.bios.2018.11.012
31. Xu Z, Dong Y, Li J, Yuan R (2015) A ferrocene-switched electrochemiluminescence "off–on" strategy for the sensitive detection of cardiac troponin I based on target transduction and a DNA walking machine. Chem Commun 51(76):14369–14372. https://doi.org/10.1039/C5CC04745E
32. Dorraj GS, Rassaee MJ, Latifi AM, Pishgoo B, Tavallaei M (2015) Selection of DNA aptamers against human cardiac troponin I for colorimetric sensor based dot blot application. J Biotechnol 208:80–86. https://doi.org/10.1016/j.jbiotec.2015.05.002
33. Wu W-Y, Bian Z-P, Wang W, Wang W, Zhu J-J (2010) PDMS gold nanoparticle composite film-based silver enhanced colorimetric detection of cardiac troponin I. Sensors Actuators B Chem 147(1):298–303. https://doi.org/10.1016/j.snb.2010.03.027
34. Chekin F, Vasilescu A, Jijie R, Singh SK, Kurungot S, Iancu M, Badea G, Boukherroub R, Szunerits S (2018) Sensitive electrochemical detection of cardiac troponin I in serum and saliva by nitrogen-doped porous reduced graphene oxide electrode. Sensors Actuators B Chem 262:180–187. https://doi.org/10.1016/j.snb.2018.01.215
35. Fan D, Bao C, Khan MS, Wang C, Zhang Y, Liu Q, Zhang X, Wei Q (2018) A novel label-free photoelectrochemical sensor based on N,S-GQDs and CdS co-sensitized hierarchical Zn2SnO4 cube for detection of cardiac troponin I. Biosens Bioelectron 106:14–20. https://doi.org/10.1016/j.bios.2018.01.050